Evidence for persistent spin fluctuations in uranium sesquicarbide

R. Eloirdi,[1,*] A. J. Fuchs,[1] J.-C. Griveau,[1] E. Colineau,[1] A. B. Shick,[1,2] D. Manara,[1] and R. Caciuffo[1]

[1]*European Commission, Joint Research Centre, Institute for Transuranium Elements, Postfach 2340, D-76125 Karlsruhe, Germany*

[2]*Institute of Physics, ASCR, Na Slovance 2, CZ-18221 Prague, Czech Republic*

(Received 25 January 2013; revised manuscript received 2 May 2013; published 13 June 2013)

The low-temperature magnetic susceptibility, heat capacity, and electrical resistivity of uranium sesquicarbide have been determined down to 2 K by combining measurements carried out on samples of U_2C_3, containing UC as minority phase, and on pure UC specimens. The presence of spin fluctuations with characteristic temperature $T_{SF} = 7$ K is revealed by a nonanalytic contribution to the specific heat behaving (well below T_{SF}) as $T^3\ln(T/T_{SF})$, and confirmed by a T^2 increase of the electrical resistivity and a $1 - \kappa T^2$ decrease of the low-temperature magnetic susceptibility. The analysis of the specific-heat data above T_{SF} provides a Debye temperature $\Theta_D \approx 256$ K and a moderate high value of the Sommerfeld coefficient, $\gamma \approx 42$ mJ mol_U^{-1} K^{-2}. The zero-temperature many-body enhancement of the electron mass is found to be $m^*/m \approx 2.7$. Our data rule out the occurrence of magnetic ordering in U_2C_3. First-principles electronic structure calculations support the absence of a magnetically ordered ground state but suggest that dynamical spin fluctuations are responsible for the electron mass enhancement.

DOI: 10.1103/PhysRevB.87.214414 PACS number(s): 71.20.Gj, 71.28.+d

I. INTRODUCTION

Mixed uranium-plutonium carbides form an important family of metallic nuclear fuels with potential advantages over conventional oxide materials thanks to a larger thermal conductivity, higher heavy-atom density, sufficiently high fusion temperature, lower equilibrium vapor pressure, and excellent structural stability.[1–4] The perspective use of carbides as fuel for propulsion system[5] and for the next generation of nuclear reactors with high operating temperature is sparking renewed interest on their physical properties.[6–10]

Three intermediate phases have been reported for the uranium-carbon system. The rocksalt NaCl-type structure exhibited by the monocarbide (UC) is stable over a narrow range of stoichiometric composition up to approximately 1100 K.[11,12] The dicarbide is substoichiometric, with composition ranging from $UC_{1.86}$ to $UC_{1.96}$;[13] below ∼2050 K, it crystallizes in the body-centered-tetragonal CaC_2-type structure (α-UC_2),[12] whereas at higher temperatures it takes the KCN-type structure (β-UC_2), isomorphous to the monocarbide.[14] The sesquicarbide U_2C_3 crystallizes in a body-centered-cubic structure, with space group $I\bar{4}3d$ and eight formula weights per unit cell.[12,15]

UC is a Fermi liquid with a large $5f$-electron spectral weight at the Fermi level.[10] Strong correlation effects among the itinerant $5f$ electrons in this material give rise to a many-body electron-mass enhancement m^*/m of about 4.[16] According to Hill,[17] for U-U spacings less than ∼3.5 Å, the $5f$ wave functions centered on adjacent atoms overlap creating a narrow band of itinerant electrons across the Fermi energy, whereas for larger distances direct overlap is prevented and the $5f$ electrons are quasilocalized. Magnetic order is usually expected only in the latter case. The U-U distance for UC is just ∼3.5 Å, and indeed this compound is a Pauli paramagnet at the edge of a magnetic instability,[18] with no localized moment and a Sommerfeld coefficient $\gamma \sim 20$ mJ mol^{-1} K^{-2}.[19,20] The tetragonal α-UC_2 is also metallic,[21] with the $5f$ electrons contributing in part to the metallic bonding and in part being transferred to the C $2p$ states.[22] The U-U distances in α-UC_2 are ∼3.54 and ∼3.90 Å, larger than the Hill limit. Nevertheless, above ∼80 K, the magnetic properties of α-UC_2 are similar to those of UC, with a practically temperature-independent susceptibility and marginal indications for very weak antiferromagnetism.[23] Data at lower temperature are not available. In U_2C_3 the U-C and the C-C bonds are weaker than those in the other carbides, which is probably the origin of its weaker thermodynamic stability and its decomposition at ∼2120 K into UC and β-UC_2.[22,24] However, metal-metal bonding stronger than in the other carbide phases is observed in U_2C_3, with the shortest U-U distance of 3.34 Å, matching the weaker metal bonds in α-uranium. The other U-U distances imposed by the U_2C_3 structure are 3.38 and 3.68 Å, slightly below and above the Hill limit. The magnetic susceptibility has been reported down to 4 K. A broad maximum observed at $T^* \sim 59$ K,[25] accompanied by a kink in the electrical resistivity,[21] was initially interpreted to signal the onset of antiferromagnetic order.[26,27] Below T^*, the electrical resistivity $\rho(T)$ increases as T^2, whereas above T^* it increases up to about 1100 K where it saturates,[21] with an overall behavior similar to the one observed for the itinerant antiferromagnet UGa_3.[28] However, no anomaly in the temperature dependence of the specific heat was observed at T^*,[29] and both neutron-diffraction[27] and ^{13}C Knight-shift measurements[30] failed to provide evidence for long-range magnetic order or for structural distortions down to 4 K. On the other hand, the broad maximum and the overall susceptibility curve at intermediate temperatures can be reproduced by a logarithmic term of the form $(T^2 + cT^4)\ln(T/\tilde{T})$.[31] A relatively high value of the Sommerfeld coefficient, $\gamma \sim 40$ mJ mol^{-1} K^{-2}, has been estimated.[29]

The picture of U_2C_3 emerging from the available experimental results bears some similarity with other compounds where the occurrence of low-temperature persistent spin fluctuations has been recognized, for instance the cubic $AuCu_3$-type USn_3 and UAl_3 compounds,[28] or the cubic Laves phase UAl_2.[32] Here, we present the results we obtained by measuring down to 2 K the magnetic susceptibility, the electrical resistivity, and the heat capacity of U_2C_3, extending to lower temperature the data already available. Below

~4 K we have observed typical fingerprints of spin-fluctuation effects, namely an enhancement of the electronic specific-heat coefficient falling off as $T^3\ln(T)$, a T^2 term in the temperature dependence of the electrical resistivity, and a parabolic temperature decrease of the magnetic susceptibility. These observations are consistent with the predictions of the spin-fluctuation theory and establish U_2C_3 as a narrow-band $5f$ paramagnetic system with low-temperature spin fluctuations.

II. EXPERIMENTAL DETAILS

The optimal route for the synthesis by arc melting of high quality samples of U_2C_3 is still controversial. The final result depends on many details, such as the grinding and pressing procedure followed for the pellet preparation, the quality of the vacuum in the furnace, or the presence of impurities coming from the electrode. Whilst UC and α-UC_2 can be obtained directly as pure compounds by arc melting, the preparation of U_2C_3 requires a subsequent high-temperature heat treatment, and it is established that the kinetic of formation prevents one from obtaining single-phase U_2C_3 samples. The final material always contains minor amounts of UC, α-UC_2, or of both phases. Nevertheless, the physical behavior of U_2C_3 can be thoroughly investigated if the amount of secondary phases present in the sample is accurately estimated. In our study, measurements of the physical properties have been performed on freshly prepared samples containing only UC as a second phase, in quantities accurately determined by Rietveld refinements of the x-ray-diffraction patterns. The UC contribution to the measured properties has been determined using the results of measurements carried out on pure UC samples, scaled to the estimated UC mass content, by assuming that the signals of the two phases add linearly.

Samples with a nominal composition of UC_x ($1.50 \leqslant x \leqslant 1.94$) were prepared by arc melting graphite (99.98%, SGL carbon, type 5300) and uranium metal under argon atmosphere (Ar 6N, 700 mbar) on a water-cooled copper hearth with a tungsten tip. To remove the oxide layer, the surface of the uranium metal ingot was electropolished in a solution of ethanol, ethylene glycol, and phosphoric acid with a composition 1:1:1. The U-C ingot was melted several times, to ensure a good homogeneity, and then broken into small pieces before being ball-milled under helium atmosphere (Retsch ball miller, type MM400, Y-stabilized ZrO_2 ball and beaker). The obtained powder, containing only UC and UC_2 according to x-ray-diffraction (XRD) analysis, was pressed at 5 GPa to get pellets of 5 mm diameter and 2 mm thickness. The pellets were packed into tantalum foils and annealed under a vacuum of 2×10^{-2} mbar at 1673 K for 40 h.

The pellets were then broken and analyzed for composition and purity by XRD and chemical analysis using combustion methods. XRD was carried out on a Bruker D8 Advance diffractometer installed inside a glove box, using Cu-$K\alpha$ radiation selected by a Ge(111) monochromator and recorded with a Lynxeye linear detector. The diffraction patterns were measured on a 2θ scan spanning the interval from 25° to 120°, with a step size of 0.009°, and a counting time of 3 s/step. All samples analyzed were two-phased, well crystallized, and containing a majority of U_2C_3 with either UC or UC_2 as a second phase. The estimate of the mass percentage of the two phases contained in the analyzed samples was obtained by Rietveld refinement of the x-ray-diffraction patterns. The quantity of U_2C_3 varied from 50 wt% up to 85 wt%. No oxide phases have been observed. As already mentioned, only samples containing UC as second phase have been used for further measurements. An upper limit of ~2 wt% for the content of UC_2 has been obtained from the statistical error on the background of the diffraction intensity in the angular region of the strong (1 0 1) UC_2 Bragg peak. The upper limit for the presence of uranium dioxide was ~3 wt%.

The overall carbon content was determined by chemical analysis using combustion under oxygen atmosphere in a high-frequency induction furnace. The produced CO was oxidized to CO_2 on a catalyst. The concentration of CO_2 was measured by infrared spectroscopy and the overall carbon content in the sample was calculated. Thus for a sample with a nominal composition of $UC_{1.5}$, after heat treatment, the chemical analysis showed a total carbon content of 6.9(2) wt%, i.e., $UC_{1.487}$. The carbon content calculated from the results of the Rietveld refinement was 6.7(1) wt%. As the difference between these two values is within the error range, no correction for free carbon content was applied.

The temperature dependence of the specific heat was measured on a Quantum Design PPMS-9 device using 14.83 mg of a sample containing 84 wt% of U_2C_3, and a sample of pure UC. Data have been collected in the temperature range 2–300 K, both in zero external magnetic field and in presence of a 9-T field. The magnetic susceptibility was measured on a Quantum Design MPMS-7 superconducting quantum interference device magnetometer, using a 34.9-mg U_2C_3-UC sample containing 50 wt% of U_2C_3. The magnetic susceptibility of UC was measured on a pure sample of 573.9 mg.

The electrical resistivity has been measured in the temperature range 1.8–300 K using a Quantum Design PPMS-9 platform and a standard four-contact dc technique. Samples with typical size $1.5 \times 0.8 \times 0.3$ mm^3 have been polished on two parallel faces to better determine the form factor. Electrical contacts have been ensured by using silver epoxy (Dupont 4929) at the contact between silver wires of 100 μm and the sample surface. The electrical current J was injected in the polished plane ($J = 5$ mA for all measurements).

III. RESULTS AND DISCUSSION

Figure 1 shows the x-ray-diffraction pattern obtained for the sample used for the specific-heat measurements. The Rietveld refinement of the measured profile reveals the presence of two cubic phases, namely 84 wt% of U_2C_3 and 16 wt% of UC. The refined lattice parameter for U_2C_3 is $a = 8.0901(6)$ Å. The unit cell contains eight formula weights, with uranium atoms located in the 16(c), $x\,x\,x$ ($x = 0.05$), and the carbon atoms in the 24(d), $x\,0\,1/4$ ($x = 0.295$) special positions. The x-ray-diffraction patterns obtained for as-cast samples of UC and UC_2 are shown in Fig. 2. For both compounds the samples are single phase, and the Rietveld refinement gives a crystallographic structure in agreement with previous reports.

Figure 3 shows the temperature dependence of the magnetic susceptibility (χ_m^{UC}) of a pure UC sample and that (χ_m^{mix}) of a two-phase sample containing UC and U_2C_3 in equal weight

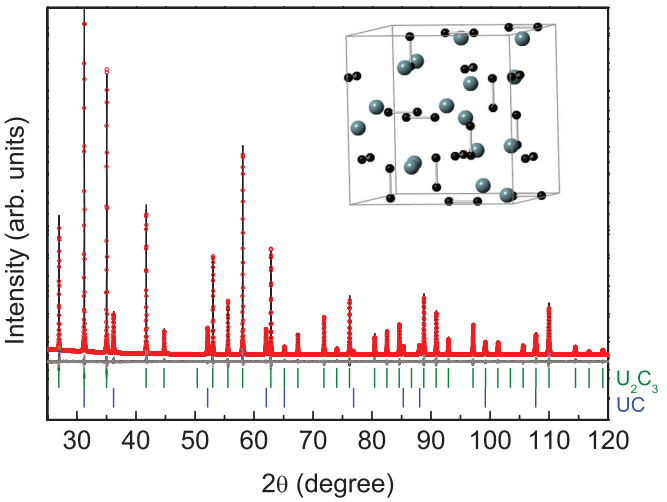

FIG. 1. (Color online) Rietveld refinement of the x-ray-diffraction pattern recorded for a sample of U_2C_3 containing UC as second phase. Red circles are observed intensities, the black solid line is the calculated diffraction profile. The green (upper) tick marks correspond to the Bragg peaks from U_2C_3 (space group $I\bar{4}3d$, no. 220), whereas the blue (lower) set refers to the UC phase. The crystallographic structure of U_2C_3 is shown in the inset.

percentage. Data have been collected in an applied field of 1 T and used to evaluate the susceptibility of a virtually pure U_2C_3 material as $[(n_{UC}+n_{U_2C_3})\chi_m^{mix}-n_{UC}\chi_m^{UC}]/n_{U_2C_3}$, where n_X is the number of moles of compound X contained in the measured sample.

UC has a Pauli paramagnetic behavior, with an almost temperature-independent value of the magnetic susceptibility $\chi_m^{UC}\sim 0.84\times 10^{-3}$ emu/mol$_U$, in good agreement with the data given by Bates *et al.*[33] The susceptibility of U_2C_3 is significantly enhanced compared to that of UC. As shown in Fig. 4, above ∼100 K it follows a Curie-Weiss behavior, with $\Theta_{CW}\sim -138$ K and an effective paramagnetic moment $\mu_{eff}=2.4(1)\mu_B$. This value is small compared with the U^{3+}

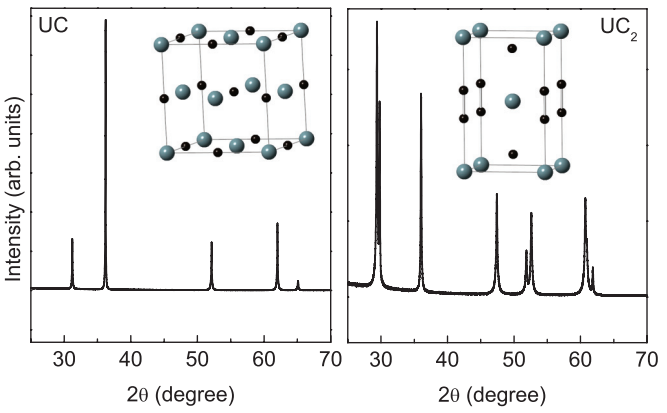

FIG. 2. (Color online) X-ray-diffraction pattern of (left panel) UC and (right panel) α-UC_2 as-cast samples obtained by arc melting. Both compounds are single phase and no impurity is detected. Insets show the crystallographic structure of the two compounds. UC crystallizes in the space group $Fm\bar{3}m$, no. 225, with $a=4.9570(2)$ Å, whereas α-UC_2 has a tetragonal $I4/mmm$ structure with $a=3.5245(3)$ Å and $c=5.9963(3)$ Å.

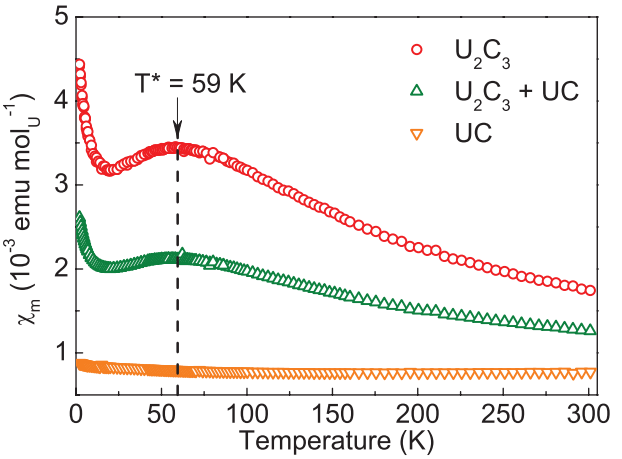

FIG. 3. (Color online) Temperature dependence of the magnetic susceptibility measured in an applied field of 1 T for (χ_m^{UC}, orange triangle) a pure UC sample and (χ_m^{mix}, green squares) a sample containing 50 wt% of U_2C_3 and 50 wt% of UC. Red circles represent the susceptibility of U_2C_3 evaluated under the assumption that χ_m^{mix} is a weighted linear combination of the susceptibilities for pure UC and U_2C_3.

ionic effective moment of $3.87\mu_B$, and could indicate either an itinerant nature of the $5f$ electrons or be an effect of the crystal field. Indeed, assuming a $5f^3$ ($^4I_{9/2}$) electronic configuration for the U ions, and C_3 site symmetry, Burton Lewis *et al.* found a value of $\mu_{eff}=2.3\mu_B$.[34] However, the information provided by a Curie-Weiss fit on a polycrystalline sample of anisotropic compound is limited, and we will not further comments on these results. With decreasing temperature, the susceptibility curve goes through a broad maximum at $T^*\sim$ 59 K. In the temperature range from about 20 to 100 K, as shown in the lower inset of Fig. 4, the experimental data

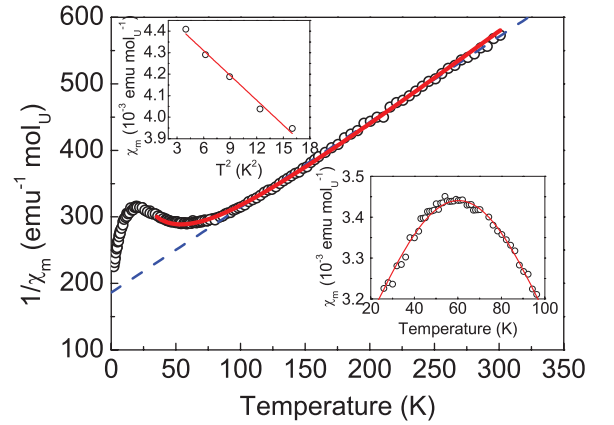

FIG. 4. (Color online) Temperature dependence of the U_2C_3 inverse magnetic susceptibility evaluated from data measured in an applied field of 1 T. The dashed blue line is the best fit to the Curie-Weiss law in the temperature range 100–300 K. The solid red line is a fit (from 34 to 300 K) to the interconfiguration fluctuation model described in the text. The lower inset shows the data measured in the interval between 20 and 100 K fitted (solid line) by a logarithmic formula given in the text. The upper inset shows the data recorded below 4 K as a function of T^2 and the fit (solid line) to a $1-\kappa T^2$ dependence.

are well represented by the logarithmic formula suggested by Misawa in the framework of the Fermi-liquid model,[31] $\chi_m = a\{1-[(T/b)^2-(T/b)^4]\ln(T/\tilde{T})\}$, with $a = 0.003$ emu/mol, $b = 118$ K, and $\tilde{T} = 129$ K. However, the observed behavior can also be reproduced by the interconfiguration fluctuation model elaborated by Sales and Wohlleben,[35] and adapted by Troć and collaborators to describe noninteger valence in uranium intermetallic compounds.[36–38] In such a model, charge fluctuations would occur between a $5f^3$ ($J = 9/2$) state and a $5f^2 6d^1$ nonmagnetic singlet originating from the excited configuration. The susceptibility is given by[38]

$$\chi(T) \propto \frac{\mu_{\rm eff}^2\left\{1-\left[1+(2J+1)\exp\left(\frac{-\Delta E}{k_B(T+T_{cf})}\right)\right]^{-1}\right\}}{k_B(T+T_{cf})}, \quad (1)$$

where ΔE is the energy difference between the two fluctuating states and $k_B T_{cf}$ is the characteristic energy for charge fluctuations. Fitting the U_2C_3 experimental data to Eq. (1) in the temperature range 35–300 K, we get $\mu_{\rm eff} \approx 1.5\mu_B$, $\Delta E \approx 249$ K, and $T_{cf} \approx 59$ K. The agreement is good, and this may suggest that fast charge fluctuations between the $5f$ and the conduction band takes place in U_2C_3, leading to a noninteger valence as also indicated by the electronic structure calculations discussed below.

We now turn to the low-temperature interval, the main focus of this work. Below ~20 K the susceptibility increases with decreasing temperature, and between 2 and 9 K the data can be fitted by $\chi_m = (4.54 - 0.037T^2)10^{-3}$ emu/mol$_U$ (upper inset of Fig. 4).

If due to a ferromagnetic impurity, the low-temperature increase of χ_m should be suppressed upon application of an external magnetic field. As shown in Fig. 5, the reduction observed at 2 K when the magnetic field is increased from 0.1 to 1 T is less than 9%, and less than 30% when the field is increased to 7 T. Above 20 K the field variation of the susceptibility curve is within experimental errors. Three field-cooled magnetization isotherms are shown in the inset of Fig. 5. At 2 K a small departure from the linear behavior is observed above ~3 T, but the residual magnetization is smaller

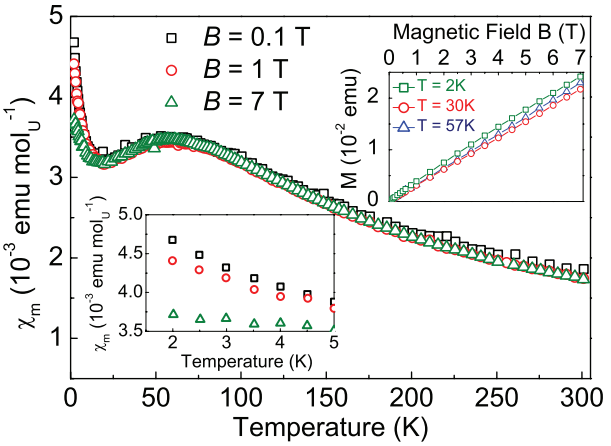

FIG. 5. (Color online) Temperature dependence of the magnetic susceptibility of U_2C_3 measured in a magnetic field of 0.1 T (black squares), 1 T (red circles), and 7 T (green triangles). The inset shows the magnetization M as a function of the magnetic field at three different temperatures.

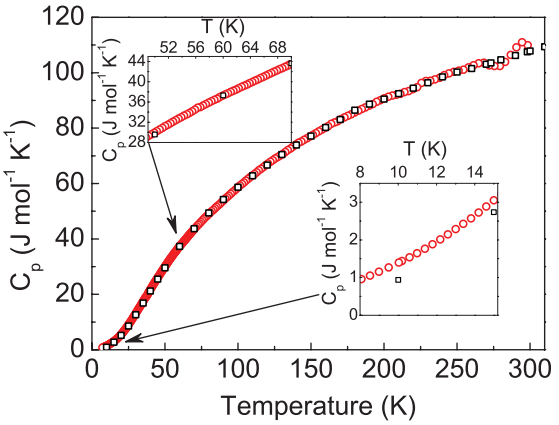

FIG. 6. (Color online) Specific heat of U_2C_3 (red circles, this study) compared with literature data (black squares, from Ref. 29). The inset shows selected temperature intervals in an expanded scale.

than the sensitivity of our instrument. Although these results cannot rule out the presence of a small amount of magnetic impurity, they suggest that the observed low-temperature upturn is associated with an intrinsic physical phenomenon. Indeed, the susceptibility of a spin fluctuation system, well below the characteristic temperature T_{SF}, is proportional to $1 - 0.13\pi^2(T/T_{SF})^2$.[39] Within this model, the fit shown in Fig. 5 would correspond to a $T_{SF} = 12.7$ K. The attribution of the low-temperature increase of the susceptibility to a physical effect is supported by the specific-heat measurements that we present below.

Figure 6 shows the zero-field temperature dependence of the specific heat of U_2C_3, obtained after subtracting the contribution of UC, representing 16 wt% of the measured sample. Our data are in very good agreement with those obtained by Andon *et al.* on a three-phase sample[29] and extend previous reports in two aspects. First, the much larger density of points in the measured curve allows us to exclude the occurrence of a phase transition, especially around $T^* = 59$ K (see top inset in Fig. 6). Second, the much lower temperature achieved allows us to study the temperature behavior below 10 K that had not been explored so far.

The scattering of data at high temperature is due to the vacuum grease we used to improve the thermal contact between the sample and the puck. At 300 K the specific heat C_p reaches a value of 110 J mol^{-1} K^{-1}, close to the Dulong and Petit value (124.7 J mol^{-1} K^{-1}), which suggests that the Debye temperature of U_2C_3 is slightly smaller than room temperature. In the following we will focus our attention on the temperature interval below 13 K. The experimental data are shown in Fig. 7 as C_p/T vs T^2, together with the corresponding curve obtained for UC.

In the temperature interval between 5 and ~13 K the experimental data can be fitted to a behavior linear in T^2, $C_p(T)/T = \gamma + \beta T^2$, where γ is the linear electronic specific-heat coefficient, determined by the band-structure electronic density of states (DOS) at the Fermi level, and βT^2 is the low-T approximation for the lattice contribution. The result of the fit provides $\gamma \sim 42$ mJ mol$_U^{-1}$ K^{-2} (per mole of U atoms) and $\beta = 0.57$ mJ mol^{-1} K^{-4}. The parameter β, when measured in units of J mol^{-1} K^{-4}, is related to the Debye

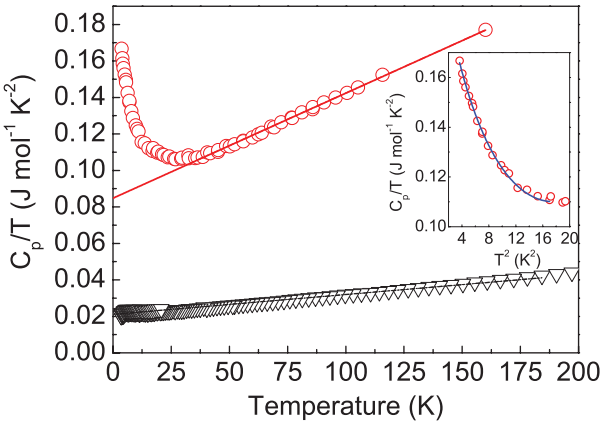

FIG. 7. (Color online) Temperature dependence of the specific heat of (red circles) U_2C_3 and (black triangles) UC, plotted as C_p/T versus T^2 for 2 < T< 13 K. Solid lines are the fit to the function $C_p/T = \gamma + \beta T^2$ in the temperature interval between 5 and ~13 K. The inset shows the low-temperature enhancement and the fit to a $T^2\ln(T)$ dependence in the interval between 2 and 4 K (blue solid line).

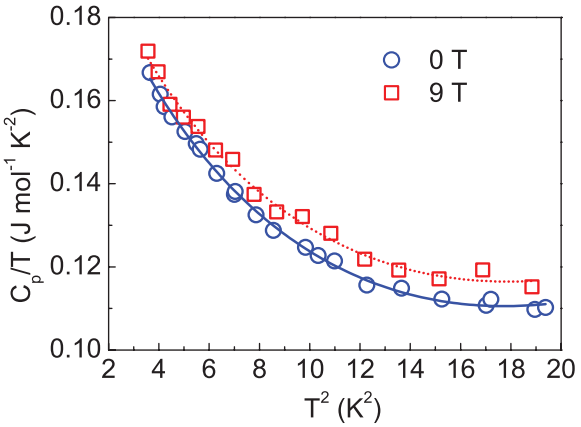

FIG. 8. (Color online) Temperature dependence of the specific heat of U_2C_3 in 0 (blue circles) and 9 T (red squares) applied magnetic fields, plotted as C_p/T versus T^2. The lines are the fit to the function $A + BT^2 + DT^2\ln(T)$.

temperature by the relation $\Theta_D = (1944n/\beta)^{1/3}$, where n is the number of atoms per formula unit (5 in the present case). We therefore obtain $\Theta_D \simeq 256$ K, in good agreement with the value of 349 K reported for the isostructural La_2C_3,[40] once the $(M_{La}/M_U)^{1/2}$ scaling factor is taken into account. For UC, we obtain $\gamma \sim 21$ mJ mol_U^{-1} K^{-2} and $\Theta_D \sim 262$ K. U_2C_3 has therefore a Sommerfeld coefficient twice as large as UC and four times larger than La_2C_3.[40] Such a relatively high γ value suggests a high density of electronic states at the Fermi energy, in agreement with x-ray photoemission spectra[41] and first-principles calculations.[22]

As shown in the inset of Fig. 7, below 5 K the specific heat increases considerably with decreasing temperature. The observed behavior reminds one of that exhibited by UAl_2, where it was interpreted as a signal for the occurrence of time-persistent, long-wavelength spin fluctuations in a Stoner-enhanced paramagnet.[32] In such a scenario, the electronic specific-heat coefficient becomes temperature dependent and assumes the form $\tilde{\gamma}(T) = \gamma[m^*/m + \alpha(T/T_{SF})^2\ln(T/T_{SF})]$,[42] where m^*/m is the effective-mass enhancement factor arising from electron-phonon interactions and from the emission and absorption of spin fluctuations, $\alpha = 6\pi^2(S-1)^2/5S$ is related to the Stoner exchange-enhancement factor S, and T_{SF} is the characteristic temperature for the spin fluctuations.

To verify if U_2C_3 can be described as a spin fluctuator system, as also suggested by the low-T magnetic susceptibility behavior, we have fitted the C_p/T data below 4 K by the relation

$$C_p/T = A + BT^2 + DT^2\ln(T), \qquad (2)$$

The results of the fit are shown in the inset of Fig. 7, and provide the values $A = \gamma m^*/m = 226(2)$, $B = \beta - \alpha\gamma\ln(T_{SF})/T_{SF}^2 = -25(1)$, and $D = \alpha\gamma/T_{SF}^2 = 12.9$ (5), when C_p is in units of mJ mol^{-1} K^{-1}. From these results, using the values of γ and β given by the fit at higher temperatures, we obtain $m^*/m = 2.7$, $T_{SF} \sim 7$ K, and $\alpha \sim 8$. The value obtained for T_{SF} is comparable with the one deduced from the analysis of the magnetic susceptibility, showing that the interpretation of the observed behaviors in terms of spin fluctuations effects is consistent. Further support is given by the data plotted in Fig. 8, demonstrating that the application of a magnetic field of 9 T does not substantially modify the upturn of C_p/T at low temperature, as predicted by the theory[39,43] (the parameters obtained by the fit of the 9-T data differ by less than half an error bar from those obtained for the zero-field curve).

Figure 9 shows the normalized electrical resistivity curve of U_2C_3 measured at zero magnetic field for two different pieces of a given batch, labeled KR298 and KR299. The data are reproducible and close to those reported by De Novion *et al.*[26] A T^2 dependence is observed at low temperature and

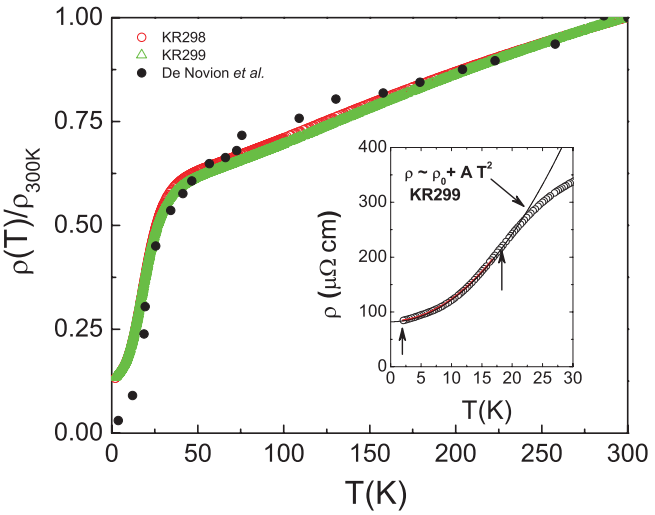

FIG. 9. (Color online) Normalized resistivity ρ/ρ_{300K} of U_2C_3 as a function of temperature at zero magnetic field for two representative samples of the same batch. The results are compared to data reported by De Novion *et al.* (Ref. 26). Inset: low-temperature dependence of the resistivity measured on sample KR299. The line is the fit to the function $\rho = \rho_0 + A_\rho T^2$, in the temperature interval indicated by the arrows.

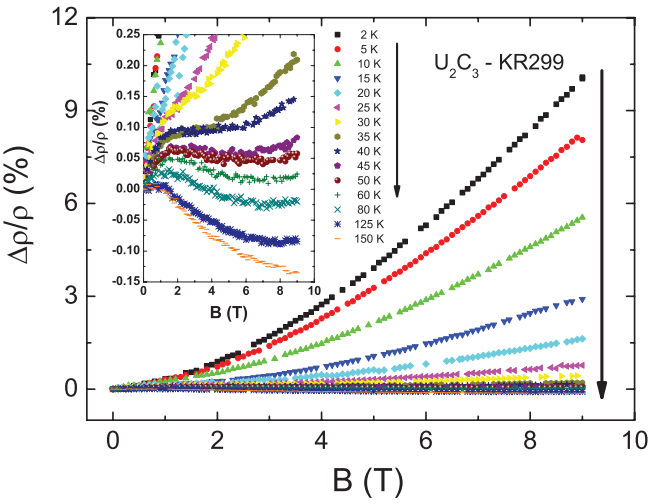

FIG. 10. (Color online) Normalized magnetoresistivity $\Delta\rho/\rho = [\rho(T,B) - \rho(T,B=0)]/\rho(T,B=0)$ of U_2C_3 as a function of magnetic field at different temperatures for sample KR299. Inset: Normalized magnetoresistivity on sample KR299 for temperature above 30 K. We observe a clear change of behavior around 80 K, with the magnetoresistivity becoming negative.

is plotted in the inset of Fig. 9 for sample KR299. A fit of the low-temperature dependence of the electrical resistivity to the formula $\rho = \rho_0 + A_\rho T^2$ gives $\rho_0 = 83\ \mu\Omega$ cm and $A_\rho = 0.4\ \mu\Omega$ cm K^{-2}. It is evident that the T^2 dependence extends up to 20 K. Above this temperature, $\rho(T)$ is linear in temperature up to an inflection point at about 40 K. The observed T^2 dependence of the low-temperature electrical resistivity is predicted by models describing spin fluctuators in the clean limit.[44] We do not observe any deviation from this T^2 dependence as predicted and reported for dirty spin fluctuations.[45,46]

Magnetoresistivity measurements have been performed on sample KR299 up to 9 T and are presented in Fig. 10. At low temperature, below 40 K, the normalized magnetoresistivity, $[\rho(T,B) - \rho(T,B=0)]/\rho(T,B=0)$, is clearly positive and achieves $\sim$10% at 2 K. With increasing temperature the magnetoresistivity decreases and becomes negative at high fields. These features are reminiscent of the behavior observed in $TiBe_2$ and UAl_2,[47] which are compounds considered as spin-fluctuator systems. The reduced effect at high field ($B = 9$ T) observed here could be explained by the huge magnetic field required to induce a significative negative contribution attributed to spin fluctuations ($B \sim 20$ T). In conclusion, measurements of transport properties support the spin-fluctuation scenario suggested already by heat-capacity results and magnetic susceptibility results.

IV. ELECTRONIC STRUCTURE CALCULATIONS

To explore further the electronic properties of U_2C_3 we have performed first-principles local-density approximation (LDA) calculations including spin-orbit (SO) coupling. We use the relativistic version of a highly accurate full-potential linearized augmented plane-wave method (FP-LAPW), in which SO coupling is included in a self-consistent second-variational procedure.[48] In the calculations we adopt the crystal structure parameters measured at room temperature. Previous work[8] shows that plain density functional theory (DFT) calculations describe quite well—within the accuracy of 1%—the crystal structure of U_2C_3. In the FP-LAPW calculations we set the radii of the atomic spheres to 2.85 a.u. (U), and 1.35 a.u. (C). The parameter $R_{Np} \times K_{\max} = 9.975$ determined the basis set size. The Brillouin zone (BZ) sampling was performed with 351 k points. Charge density self-consistence is achieved to $0.5\times10^{-4} e/(\text{a.u.})^3$.

The total density of states (TDOS), and f-state partial DOS (fDOS) are shown in Fig. 11(a). The DOS near the Fermi energy (E_F) has mostly U-f character, with a sharp $j = 5/2$ peak located at the E_F edge. The C-s states are located at the bottom of the valence band at 6–8 eV below E_F, and p states are spread all over the valence band [see Fig. 11(b)], with the

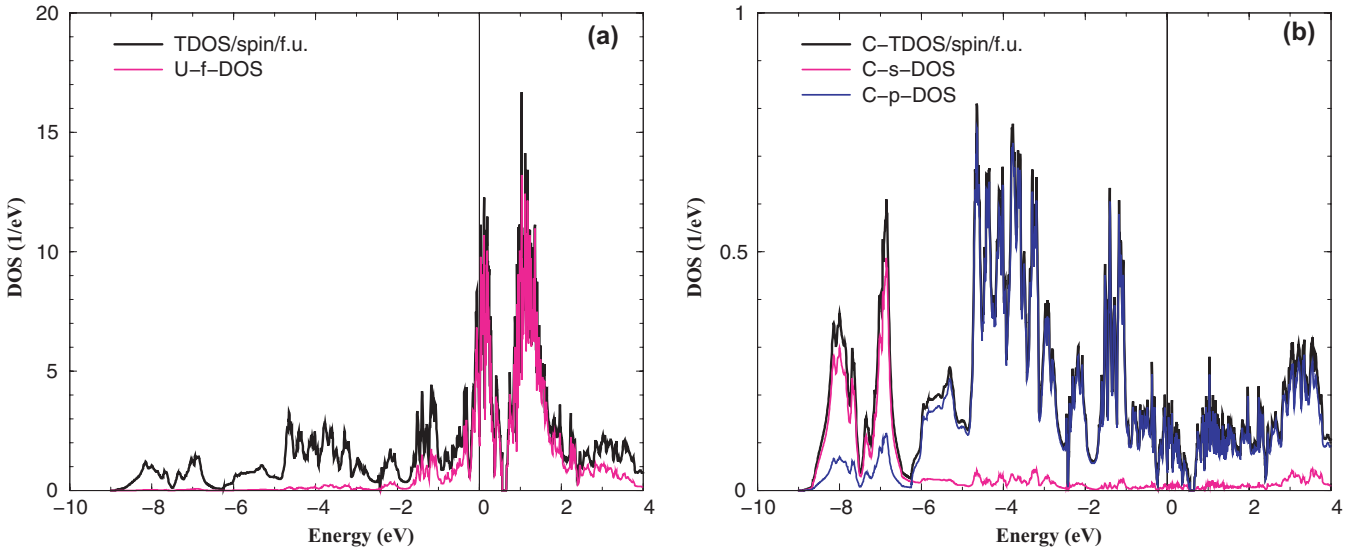

FIG. 11. (Color online) Total (TDOS) and the U atom f-electron (fDOS) density of states for U_2C_3 (a), C-atom total (C-TDOS), s- and p-states DOS (b).

DOS maximum at ≈4 eV below E_F. This indicates essential hybridization between C-p and U-f states.

The resulting TDOS at E_F of 5.8 states/eV/f.u. corresponds to the noninteracting value of the Sommerfeld coefficient $\gamma \sim 14$ mJ/K^2/mol, which is substantially lower than the experimental value of 42 mJ/K^2/mol. However, the theoretical value of the Sommerfeld coefficient is expected to increase due to the electron mass enhancement caused by dynamical electron interactions and electron-phonon coupling.

We estimate the electron-phonon coupling $\lambda_{\rm tr}$ from the Bloch-Grüneisen transport theory, assuming that at sufficiently high temperatures $T \geqslant 0.7 \times \Theta_D$, i.e., above 180 K in the case of U_2C_3, the temperature dependence of electrical resistivity is only due to electron-phonon interactions. Next, we employ an approximate expression,[49] that relates the electrical resistivity ρ and the electron-phonon coupling strength. Calculating the Drude plasma energy $\Omega_p = 0.822$ eV, and taking the experimental resistivity at $T = 300$ K of ≈624 $\mu\Omega$ cm (minus the residual value ≈84 $\mu\Omega$ cm), we get $\lambda_{\rm tr} = 0.33$.

Thus, the electron-phonon coupling alone cannot explain the difference between the experimental $\gamma_{\rm exp}$ and the LDA calculated Sommerfeld coefficient $\gamma_{\rm LDA}$ ($\gamma_{\rm exp}/\gamma_{\rm LDA} = 3.1$). Writing $\gamma = \frac{\pi^2}{3} k_B^2 N(E_F) m^*/m$, and removing the electron-phonon coupling, we estimate the effective-mass enhancement $m^*/m = 2.8$ due to dynamical electron correlations. This value of mass enhancement is in surprisingly good agreement with the value derived from the analysis of the experimental data based on the assumption of dynamical Stoner-like spin fluctuations, as discussed above.

As follows from our calculations, LDA gives the Stoner parameter $I = 34$ meV, and the product IN(E_F)/(per spin) = $0.39 < 1$ so that U_2C_3 is far from a magnetic instability. This yields the Stoner enhancement $S = [1 - {\rm IN}(E_F)]^{-1} = 1.65$, and $\alpha = 3.03$. Thus the ratio of experimental to LDA estimated values of α is equal to 2.7, close to the effective-mass enhancement. This gives us the reason to suggest that dynamical spin fluctuations are responsible for the enhancement of the electronic specific-heat coefficient. These dynamical fluctuations are not accounted for either in our LDA calculations or in previous calculations of Ref. 8. The LDA/GGA+U nonrelativistic calculations[22] constrained to paramagnetic phase do not include these effects as well.

In order to estimate the effect of dynamical Coulomb correlations, we calculate the LDA Green's function,

$$[G_{\rm LDA}(z)]_{\gamma_1\gamma_2} = \frac{1}{V_{\rm BZ}} \int_{\rm BZ} d^3k [z + \mu - H_{\rm LDA}(\mathbf{k})]^{-1}_{\gamma_1\gamma_2}. \qquad (3)$$

where $\gamma = (m\sigma)$ label f spin orbitals on the U atom site. Next, we calculate the lattice site-diagonal self-energy $\Sigma(z)$ which contains the electron-electron correlations. The effective multiorbital impurity Hamiltonian for the complete seven-orbital f shell including the full spherically symmetric Coulomb interaction and spin-orbit coupling[50] is used,

$$H = \sum_{\substack{kmm'\\ \sigma\sigma'}} [\epsilon^k]^{\sigma\sigma'}_{mm'} b^\dagger_{km\sigma} b_{km'\sigma'} + \sum_{m\sigma} \epsilon_f f^\dagger_{m\sigma} f_{m\sigma}$$
$$+ \sum_{mm'\sigma\sigma'} \xi(\mathbf{l}\cdot\mathbf{s}) f^\dagger_{m\sigma} f_{m'\sigma'}$$
$$+ \sum_{\substack{kmm'\\ \sigma\sigma'}} \left([V^k]^{\sigma\sigma'}_{mm'} f^\dagger_{m\sigma} b_{km'\sigma'} + {\rm H.c.}\right)$$
$$+ \frac{1}{2} \sum_{\substack{mm'm''\\ m'''\sigma\sigma'}} U_{mm'm''m'''} f^\dagger_{m\sigma} f^\dagger_{m'\sigma'} f_{m'''\sigma'} f_{m''\sigma}, \qquad (4)$$

where $f^\dagger_{m\sigma}$ creates an electron in the f shell and $b^\dagger_{m\sigma}$ creates an electron in the "bath" which consists of those host-band states that hybridize with the impurity f shell. Diagonalization is performed making use of the finite-temperature "exact diagonalization" (ED) method.[51] Note that for the ED method to be applicable, the continuum of the bath states is discretized.

In order to specify the bath parameters, we assume that LDA represents the noninteracting model for U_2C_3, and associate with it the solution of Eq. (4) without the last Coulomb-interaction term. Moreover, we assume that the first and third terms in Eq. (4) are diagonal in $\{j, j_z\}$ representation, and that the only essential hybridization occurs in the vicinity of E_F. Next, we obtain $V_{k=1}^{j=5/2,7/2}$ from the LDA hybridization function $\Delta = \frac{1}{\pi N_f} {\rm Im\,Tr}[G^{-1}(\epsilon + i\delta)]$ (0.18 eV for $j = 5/2$, $N_f = 6$, and 0.21 eV for $j = 7/2$, $N_f = 8$), and adjust $\epsilon_{k=1}^{5/2,7/2}$ to approximately reproduce LDA values for 5f-states occupations $n_f^{5/2} = 1.30$ and $n_f^{7/2} = 1.26$.

At last, the local Green's function $G(z)$ is calculated,

$$[G(z)]^{-1}_{\gamma_1\gamma_2} = [G_{\rm LDA}(z)]^{-1}_{\gamma_1\gamma_2} - \Delta\epsilon\, \delta_{\gamma_1\gamma_2} - [\Sigma(z)]_{\gamma_1\gamma_2}, \qquad (5)$$

where $\Delta\epsilon$ accounts for the difference between the impurity and the lattice chemical potentials, for the number of f electrons $n_f = 2.56$ fixed to the LDA value.

The resulting f-orbital DOS [spectral function, $N(E)$] is shown in Fig. 12. Comparison with LDA-DOS [see Fig. 11(a)] shows that the electron correlations have rather a moderate effect on the occupied part of the spectra. The unoccupied part

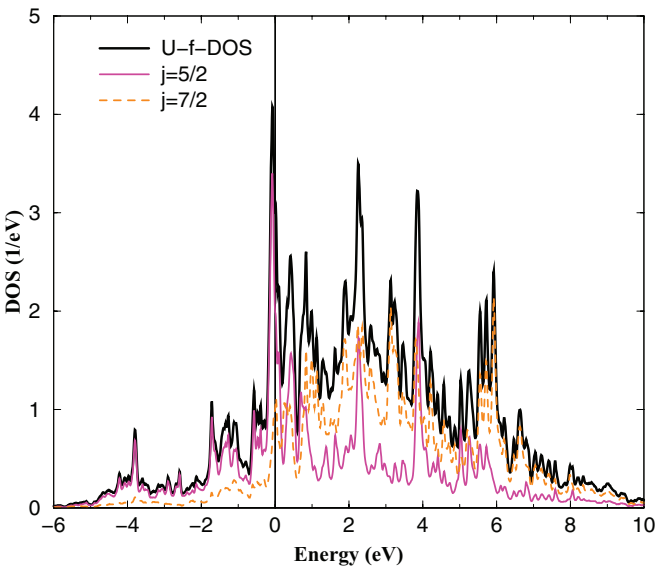

FIG. 12. (Color online) The U atom spectral density of states (total and $j = 5/2,7/2$ projected) as a result of LDA+"exact diagonalization" calculations.

of the f manifold is modified substantially due to transitions to higher multiplets.

We estimate an f contribution to electronic specific-heat coefficient $\gamma = \frac{\pi^2}{3} k_B^2 \mathrm{Tr}[N(E_F)(1 - \frac{d\Sigma(\omega)}{d\omega})|_{\omega=0}]$ of $\approx$ 31.4 mJ/K^2/mol, which compares well with the experimental value of 42 mJ/K^2/mol. This improvement on the γ value prediction is due to the effective-mass enhancement calculated from a quasiparticle weight Z as $m^*/m = Z^{-1} = \mathrm{Tr}[N(E_F)(1 - \frac{d\Sigma(\epsilon)}{d\epsilon})|_{\epsilon=E_F}]/\mathrm{Tr}[N(E_F)]$. The $m^*/m \approx 2.21$ is in reasonable agreement with the mass enhancement value of 2.7, derived from the analysis of the experimental data. It is somewhat smaller than the $m^*/m = 3.7$ reported in Ref. 10 for UC on the basis of dynamical mean-field theory (DMFT) calculations. It is consistent with the view that the effects of dynamical electron correlations are stronger in UC than in U_2C_3. Indeed, our calculations serve rather as an estimate, and complete self-consistent DMFT calculations are needed. Due to the complex (as compared to UC) crystal structure with 20 atoms in the asymmetric portion of the unit cell, these calculations are left for future consideration.

V. CONCLUSION

Two-phase samples of U_2C_3 mixed with UC have been obtained in a reproducible way by arc melting of the constituent elements followed by a thermal treatment at 1673 K. The magnetic susceptibility, specific heat, and electrical resistivity have been measured on the mixed material and on pure UC samples, in order to extract intrinsic quantities for U_2C_3. By extending previous measurements down to 2 K, we have found evidence for time-persistent spin fluctuations with a characteristic temperature $T_{SF} = 7$ K, which produce a temperature-dependent renormalization of the electronic specific-heat coefficient, decaying as $T^2\ln(T)$, a decrease of the low-T magnetic susceptibility as $1 - \kappa T^2$, and a T^2 increase of the low-temperature electrical resistivity. The relatively large Sommerfeld coefficient, $\gamma = 42$ mJ mol$_U^{-1}$(U) K^{-2}, with a many-body mass enhancement at zero-temperature $m^*/m \approx 2.7$, suggests a high density of electron states of $5f$ parentage at the Fermi level, as confirmed by LDA and LDA+ exact diagonalization electronic structure calculations. The magnetic susceptibility shows a broad maximum at 59 K, and between ~25 and 300 K can be fitted by a phenomenological relation that has been used to describe mixed valency in intermetallic uranium compounds.[38] We have found no indications of long-range magnetic order down to 2 K and we propose that U_2C_3 is a compound supporting magnetic fluctuations with low excitation energies. Nuclear magnetic resonance measurements of the spin-lattice relaxation rate would be useful to determine directly the characteristic energy scale of the persistent spin fluctuations, as done for instance for the $NpPd_5Al_2$ unconventional superconductor.[52,53]

ACKNOWLEDGMENTS

We are grateful to D. Bouëxière, G. Pagliosa, and P. Amador for technical support, and to S. Morel and K. Casteleyn who performed the carbon content analysis. A.B.S. acknowledges financial support from Czech Republic Grant No. GACR P204/10/0330.

*Corresponding author: rachel.eloirdi@ec.europa.eu

[1] Hj. Matzke, *Science of Advanced LMFBR Fuels* (North-Holland, Amsterdam, 1986).
[2] R. W. Stratton, G. Ledergerber, F. Ingold, T. W. Latimer, and K. M. Chidester, J. Nucl. Mater. **204**, 39 (1993).
[3] D. C. Crawford, D. L. Porter, and S. L. Hayes, J. Nucl. Mater. **371**, 202 (2007).
[4] D. Petti, D. Crawford, and N. Chauvin, MRS Bull. **34**, 40 (2009).
[5] D. R. Koenig, Los Alamos National Laboratory Report No. LA-10062-H, UC-33, May 1986.
[6] C. Utton, F. De Bruycker, K. Boboridis, R. Jardin, H. Noel, C. Gueneau, and D. Manara, J. Nucl. Mater. **385**, 443 (2009).
[7] L. Biasetto, P. Zanonato, S. Carturan, P. Di Bernardo, P. Colombo, A. Andrighetto, and G. Prete, J. Nucl. Mater. **404**, 68 (2010).
[8] M. Freyss, Phys. Rev. B **81**, 014101 (2010).
[9] C. Guéneau, N. Dupin, B. Sundman, C. Martial, J.-C. Dumas, S. Gossé, S. Chatain, F. De Bruycker, D. Manara, and R. J. M. Konings, J. Nucl. Mater. **419**, 145 (2011).
[10] Q. Yin, A. Kutepov, K. Haule, G. Kotliar, S. Y. Savrasov, and W. E. Pickett, Phys. Rev. B **84**, 195111 (2011).
[11] R. Rundle, N. Baenziger, A. Wilson, and R. McDonald, J. Am. Chem. Soc. **70**, 99 (1948).
[12] A. E. Austin, Acta Crystallogr. **12**, 159 (1959).
[13] E. K. Storms, *The Refractory Carbides* (Academic, New York, 1967), pp. 174–182.
[14] A. L. Bowman, G. P. Arnold, W. G. Witteman, T. C. Wallace, and N. G. Nereson, Acta Crystallogr. **21**, 670 (1966).
[15] J. F. A. Hennecke and C. J. Toussaint, J. Appl. Crystallogr. **2**, 301 (1969).
[16] J. T. Ito, H. Kumigashira, T. Takahashi, E. Yamamoto, Y. Haga, and Y. Ōnuki, J. Magn. Magn. Mater. **226–230**, 40 (2001).
[17] H. H. Hill, in *Plutonium 1970 and Other Actinides*, edited by W. N. Miner, Nuclear Metallurgy, Vol. 17 (AIME, New York, 1970), pp. 2–19.
[18] M. B. Brodsky, Rep. Prog. Phys. **41**, 1547 (1978).
[19] A. de Combarieu, P. Costa, and J.-C. Michel, C. R. Acad. Sci. Paris **256**, 5518 (1963).
[20] J. Harness, J. Matthews, and N. Morton, Brit. J. Appl. Phys. **15**, 963 (1964).
[21] H. Matsui and M. Tamaki, J. Phys. Chem. Solids. **41**, 351 (1980).
[22] H. Shi, P. Zhang, S.-S. Li, B. Wang, and B. Sun, J. Nucl. Mater. **396**, 218 (2010).
[23] B. T. Matthias, C. W. Chu, E. Corenzwit, and D. Wohlleben, Proc. Natl. Acad. Sci. USA **64**, 459 (1969).
[24] R. Benz and D. Farr, J. Nucl. Mater. **42**, 217 (1972).
[25] G. Raphael and C. H. de Novion, Solid State Commun. **7**, 791 (1969).
[26] C. H. De Novion, P. Costa, and G. Dean, Phys. Lett. **19**, 455 (1965).
[27] C. H. De Novion, J. P. Krebs, and L. P. Meriel, C. R. Acad. Sci. Paris Ser. B **263**, 457 (1966).

[28] A. L. Cornelius, A. J. Arko, J. L. Sarrao, J. D. Thompson, M. F. Hundley, C. H. Booth, N. Harrison, and P. M. Oppeneer, Phys. Rev. B **59**, 14473 (1999).
[29] R. J. L. Andon, J. F. Counsell, J. F. Martin, and H. J. Hedger, Trans. Faraday Soc. **60**, 1030 (1964).
[30] J. L. Boutard and C. H. de Novion, Solid State Commun. **14**, 181 (1974).
[31] S. Misawa, Solid State Commun. **16**, 1215 (1974).
[32] R. J. Trainor, M. B. Brodsky, and H. V. Culbert, Phys. Rev. Lett. **34**, 1019 (1975).
[33] L. F. Bates and P. B. Unstead, Br. J. Appl. Phys. **15**, 543 (1964).
[34] W. Burton Lewis, S. W. Rabideau, N. H. Krikorian, and W. G. Witteman, Phys. Rev. **170**, 455 (1968).
[35] B. C. Sales and D. K. Wohlleben, Phys. Rev. Lett. **35**, 1240 (1975).
[36] R. Troć, Physica B **378–380**, 985 (2006).
[37] R. Troć, J. Alloys Compd. **442**, 34 (2007).
[38] R. Troć, M. Pasturel, O. Tougait, M. Potel, and H. Noël, Intermetallics **19**, 913 (2011).
[39] M. T. Béal-Monod, S. K. Ma, and D. R. Fredkin, Pyhs. Rev. Lett. **20**, 929 (1968).
[40] J. S. Kim, W. Xie, R. K. Kremer, V. Babizhetskyy, O. Jepsen, A. Simon, K. S. Ahn, B. Raquet, H. Rakoto, J. M. Broto, and B. Ouladdiaf, Phys. Rev. B **76**, 014516 (2007).
[41] M. Eckle, R. Eloirdi, T. Gouder, M. Colarieti Tosti, F. Wastin, and J. Rebizant, J. Nucl. Mater. **334**, 1 (2004).
[42] S. Doniach and S. Engelsberg, Phys. Rev. Lett. **17**, 750 (1966).
[43] W. F. Brinkman and S. Engelsber, Phys. Rev. **169**, 417 (1968).
[44] B. Coqblin, J. R. Iglesias-Sicardi, and R. Jullien, Contemp. Phys. **19**, 327 (1978), and references therein.
[45] P. S. Riseborough, Phys. Rev. B **29**, 4134 (1984).
[46] M. S. Wire and A. L. Giorgi, Phys. Rev. B **32**, 1687 (1985).
[47] J. M. van Ruitenbeek, A. P. J. van Deursen, H. W. Myron, A. J. Arko, and J. L. Smith, Phys. Rev. B **34**, 8507 (1986).
[48] A. B. Shick, D. L. Novikov, and A. J. Freeman, Phys. Rev. B **56**, R14259 (1997).
[49] P. B. Allen, Phys. Rev. B **36**, 2920 (1987).
[50] A. B. Shick, J. Kolorenc, V. Janiš, and A. I. Lichtenstein, Phys. Rev. B **84**, 113112 (2011).
[51] J. Kolorenc, A. I. Poteryaev, and A. I. Lichtenstein, Phys. Rev. B **85**, 235136 (2012).
[52] H. Chudo, H. Sakai, Y. Tokunaga, S. Kambe, D. Aoki, Y. Homma, Y. Shiokawa, Y. Haga, S. Ikeda, T. D. Matsuda, Y. Ōnuki, and H. Yasuoka, J. Phys. Soc. Jpn. **77**, 083702 (2008).
[53] G. A. Ummarino, R. Caciuffo, H. Chudo, and S. Kambe, Phys. Rev. B **82**, 104510 (2010).